energies

MDPI

Article

Electrical Tree Initiation and Growth in Silicone Rubber under Combined DC-Pulse Voltage

Tao Han, Boxue Du * and Jingang Su

Key Laboratory of Smart Grid of Education Ministry, School of Electrical and Information Engineering, Tianjin University, Tianjin 300072, China; hant@tju.edu.cn (T.H.); sujg1357@126.com (J.S.)

* Correspondence: duboxue@tju.edu.cn; Tel.: +86-22-2740-5477

Received: 12 February 2018; Accepted: 26 March 2018; Published: 28 March 2018

Abstract: Electrical tree is a serious threat to silicone rubber (SIR) insulation and can even cause breakdown. Electrical trees under alternating current (AC) and direct current (DC) voltage have been widely researched. While there are pulses in high-voltage direct current (HVDC) cables under operating conditions caused by lightning and operating overvoltage in the power system, little research has been reported about trees under combined DC-pulse voltage. Their inception and growth mechanism is still not clear. In this paper, electrical trees are studied under several types of combined DC-pulse voltage. The initiation and growth process was recorded by a digital microscope system. The experimental results indicate that the inception pulse voltage is different under each voltage type and is influenced by the combined DC. The initial tree has two structures, determined by the pulse polarity. With increased DC prestressing time, tree inception pulse voltage with the same polarity is clearly decreased. Moreover, a special initial bubble tree was observed after the prestressing DC.

Keywords: combined DC-pulse voltage; silicone rubber; electrical tree; inception voltage; tree structure; prestress

1. Introduction

High-voltage direct current (HVDC) cable is an important way to carry out large-capacity, long-distance and low-loss power transmission [1,2]. Cable accessories are not only an important part of the HVDC cable system but also the weakest link, where most cable insulation failure occurs [3]. The reason is that the internal insulation structure of cable accessories is composed of multilayer solid insulation, which contains cross-linked polyethylene (XLPE), silicone rubber (SIR) and so forth. The different conductivities of insulating materials lead to a complex accumulation of space charges and serious electric field distortion, which can lead to insulation aging [4–6]. It is necessary to study the insulation and breakdown of cable accessories to ensure the safe and stable operation of HVDC cable systems.

The aging of insulation in cable accessories is a gradual process. Electrical tree is the main reason for insulation aging and breakdown [5–10]. In the study of alternating current (AC) trees, a number of models have been proposed, while there is no alternating electric field under DC voltage and most models are not suitable. Research on DC trees is mainly focused on the following aspects: (1) initiation mechanism and morphological characteristics of electrical trees at different DC voltage levels [11–15]; and (2) grounded DC trees [15–20]. It has been confirmed that DC trees are difficult to initiate, so impulse and AC voltage have been employed to trigger an initial tree before applying DC voltage [18,21,22]. Meanwhile, trapping and detrapping space charges have been found to be important in grounded DC trees. During the growth process, it has been found that the growth speed of DC trees is polarity-dependent and partial discharge is supposed to be the driving force,

which is similar to AC trees [18,22]. However, the following pulse voltages exist in HVDC cables under operating conditions: (1) lightning impulse voltage introduced by the overhead line [23–25]; and (2) operating impulse voltage caused by line fault [25]. It is noteworthy that these pulse voltages will be combined with the DC voltage in HVDC cables, causing the line voltage to change abruptly and intensifying the electric field distortion [26–28]. Under this type of voltage, the voltage polarity in the cable may be much higher than the operating voltage or even turn to heteropolarity. At present, there is little research on electrical trees under combined DC-pulse voltage. Their initiation and growth mechanism is still not clear, which limits the development of HVDC cable accessories.

SIR is a widely used insulating material in cable accessories, because it is easy to install and has excellent electrical properties [29]. Research on electrical trees in SIR have been focused on AC trees and pulse trees; temperature, mechanical stress and frequency have also been considered [30–32]. However, electrical tree characteristics under combined DC-pulse voltage are still not clear because of the different space charge dynamic characteristics under this voltage.

In this paper, combined voltages were applied on SIR samples through typical needle-plate electrodes to initiate electrical trees. The tree inception and growth process was observed by a digital microscope system. The research indicates that the treeing characteristics in SIR under combined DC-pulse voltage are dependent on both DC and pulse. The initiation mechanism is analyzed and the effect of prestressing DC is discussed.

2. Experiment

2.1. Test Samples and Electrode Arrangement

SIR samples were prepared as follows. At first, the mold was made of glass, with the internal dimension of 30 mm × 15 mm × 3 mm. Then the liquid SIR was injected into the mold. After this, a needle with a curvature radius of 3 μm was fixed in the mold. The needle was picked by using a microscope before it was employed. The distance from the needle tip to the edge of the mold was set at 2 mm. To degas the sample, it was put into the vacuum tank for 120 min. Finally, 10 days of vulcanization was carried out at 20 °C. The sample setup is shown in Figure 1. The dimensions of the samples were 30 mm × 15 mm, with a thickness of 3 mm. Copper foil was attached to the bottom of the samples and grounded in the experiment, the distance between needle and ground electrode was 2 mm. Before the experiment, all the samples were checked by using the microscope and samples with an air gap on the needle tip were abandoned to avoid errors.

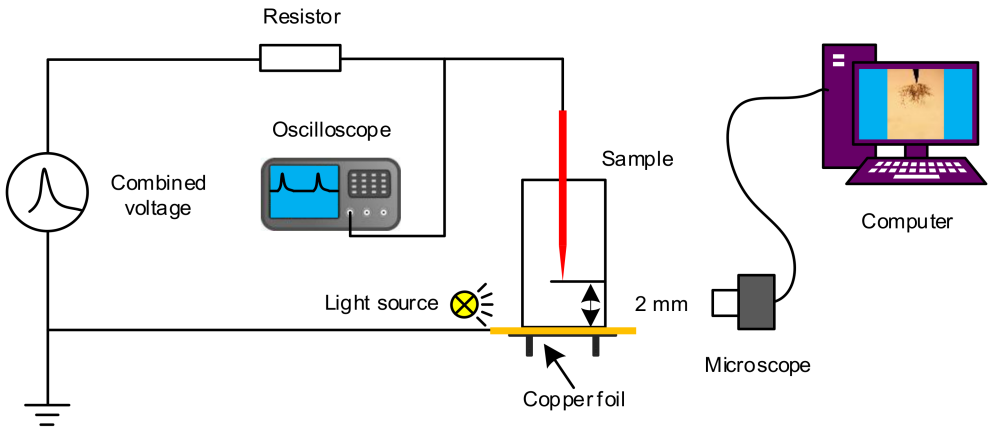

Figure 1. Schematic diagram of experimental setup.

2.2. Experimental Apparatus and Procedure

The experimental setup is shown in Figure 1. The combined voltage was generated by a combined power source containing DC (manufactured by Dongwen High Voltage Power Co., Ltd., Tianjin,

China, models DW-N503-1ACDF and DW-P503-1ACDF) and pulse power (manufactured by HV lab of Tianjin University, model PPS20D). The DC voltage amplitude ranged from −20 to +20 kV and the repetitive pulse voltage amplitude ranged from −20 to +20 kV. During the experiment, DC voltage was applied to the needle electrode first. Then pulse voltage was applied and the combined DC-pulse electric field was generated. The voltage waveform could be observed by the oscilloscope (TDS3032b, Tektronix, Beaverton, OR, USA). A digital microscope (XDC10A, Shenzhen Sangnond Technology Co., Ltd., Shenzhen, China) and computer were employed to record the growth process of electrical trees. The experimental temperature was 20 °C, the pressure was 0.1 Mpa and humidity was 35%.

During the experiment, 4 types of voltage were applied to the samples. Typical pulse voltage and combined voltage with negative DC are shown in Figure 2. The voltage types are defined as follows: (1) type A: pulse without DC, as shown in Figure 2a; (2) type B: pulse and DC in the same polarity, as shown in Figure 2b; (3) type C: pulse and DC in heteropolarity, without zero potential in the whole voltage waveform, as shown in Figure 2c; and (4) type D: pulse and DC in heteropolarity, with zero potential in the voltage waveform, as shown in Figure 2d. Combined voltage with positive DC is similarly defined. As shown in Figure 2b, the peak value is the highest voltage at the peak of type B voltage. The phase when the voltage is beyond 0 is defined as positive phase and otherwise is defined as negative phase, as shown in Figure 2d. Twenty samples under each type of voltage were tested.

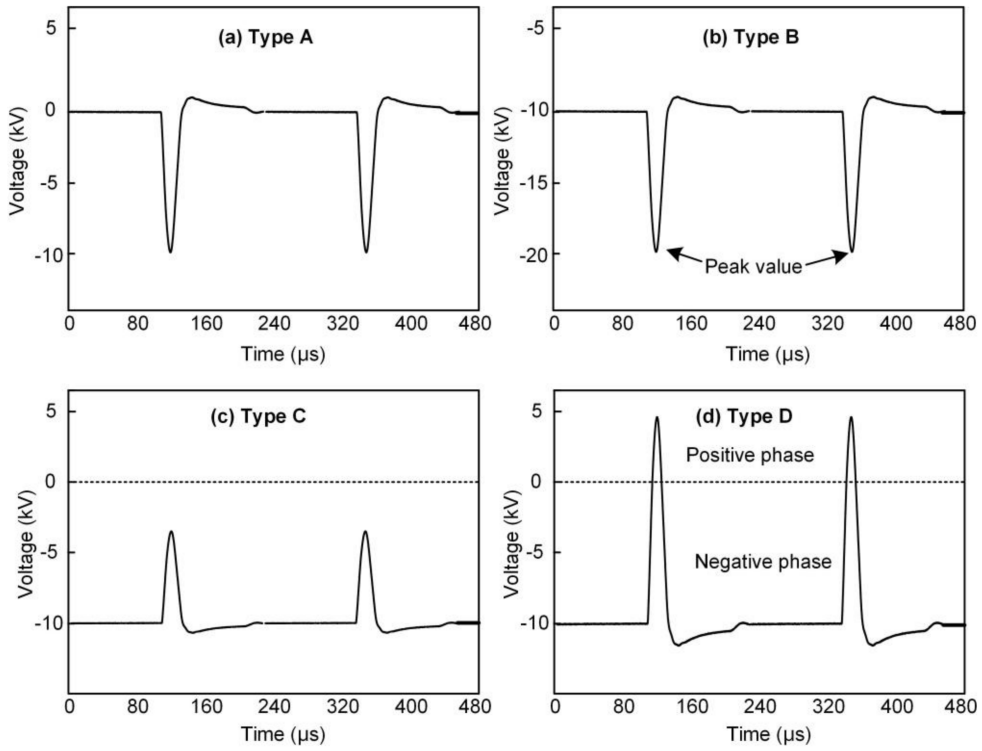

Figure 2. Different types of combined direct current (DC)-pulse voltage with negative DC: (**a**–**d**) typical combined voltage of types A, B, C and D, respectively.

3. Results

3.1. Tree Inception under Combined Voltage

3.1.1. Initial Pulse Voltage

The inception characteristics of electric trees under different voltages was tested. In the test, DC voltage was applied first, then pulse voltage was increased by 1 kV/step. Voltage remained for 30 s at each step to observe whether a tree was initiated. If an electric tree with a length of more than

20 μm was generated, the tree was considered to be initiated. The inception voltage was recorded and is shown in Figure 3. It was found that with changing DC voltage, inception pulse voltage obviously varied. When the polarities of DC and pulse were different, the inception pulse voltage increased with DC, while with the same polarity, there was no obvious change in the inception pulse voltage.

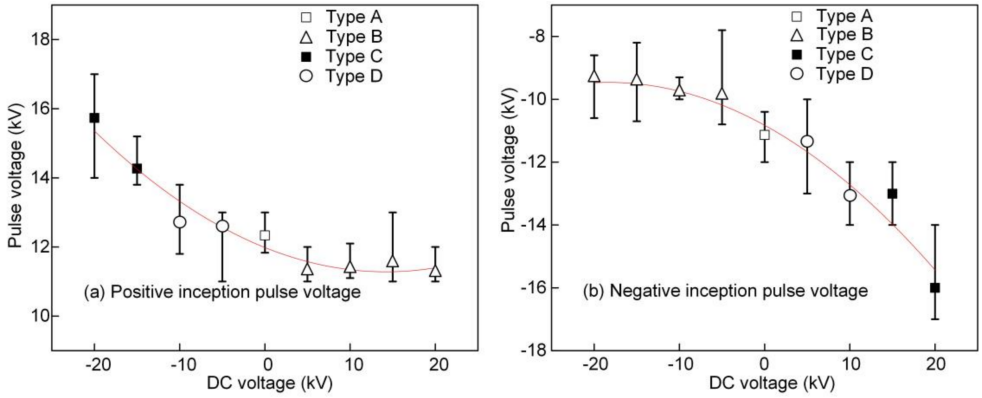

Figure 3. Tree inception pulse voltage with different DC: (**a**) positive inception pulse voltage; (**b**) negative inception pulse voltage.

3.1.2. Structure of Initial Tree

During the inception process, two types of initial trees were seen. The initial tree structure at 0.5 s is shown in Figure 4. It is obvious that the inception tree structure was related to the polarity of the pulse voltage. When the pulse voltage was positive, the inception tree was in the structure of more than 3 channels, while under negative pulse it only had 1 channel. The reason will be discussed in the following sections.

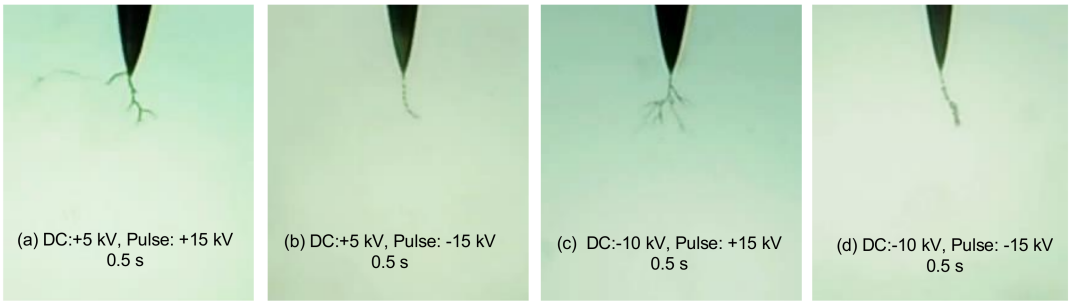

Figure 4. Initial tree structure under different combined voltage: (**a**) +5 kV DC and +15 kV pulse; (**b**) +5 kV DC and −15 kV pulse; (**c**) −10 kV DC and +15 kV pulse; (**d**) −10 kV DC and −15 kV pulse.

3.2. DC Prestressed Tree

Trees with different DC prestressing times were initiated during the experiment. Prestressing time means the stressing time of DC before the pulse voltage is combined. The inception pulse voltages and tree structures with different prestressing times were recorded.

3.2.1. Inception Pulse Voltage with Different Prestressing Times

As shown in Figure 5, inception pulse voltages with different DC prestressing times were recorded. The DC voltage was ±15 kV. The prestressing times were 0, 10 and 60 min. When the DC voltage was −15 kV, the average negative inception pulse voltage decreased from −10.5 to −8 kV at 10 min and −6 kV at 60 min. However, there was no significant change in average positive pulse voltage. When the DC voltage was +15 kV, this significant decrease only occurred with positive inception pulse

voltage. It was found that the inception pulse voltage changed when it had the same polarity as the prestressing DC.

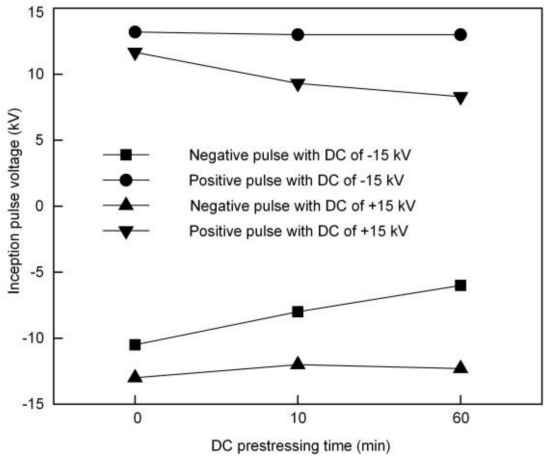

Figure 5. Inception pulse voltage with different DC prestressing times.

3.2.2. Initial Bubble Tree

During the experiment, it was found that a special initial tree with a bubble structure appeared when the prestressing was 10 min or longer. Figure 6 shows the initial stage of a bubble tree under the combined voltage of 15 kV DC and positive pulse. The bubble appeared after the pulse voltage was increased to 7 kV and its length kept constant while the pulse voltage was under 12 kV. In this process, the length of the bubble tree was about 50 µm. However, when the pulse voltage increased to 12 kV, the bubble broke and a typical branch tree was generated from the bubble edge. The bubble tree shrank to be smaller than its previous volume. After this, the tree grew as a normal branch tree. This type of bubble tree was not observed under combined voltage without prestressing DC. It is obvious that long prestressing time leads to the occurrence of a bubble tree.

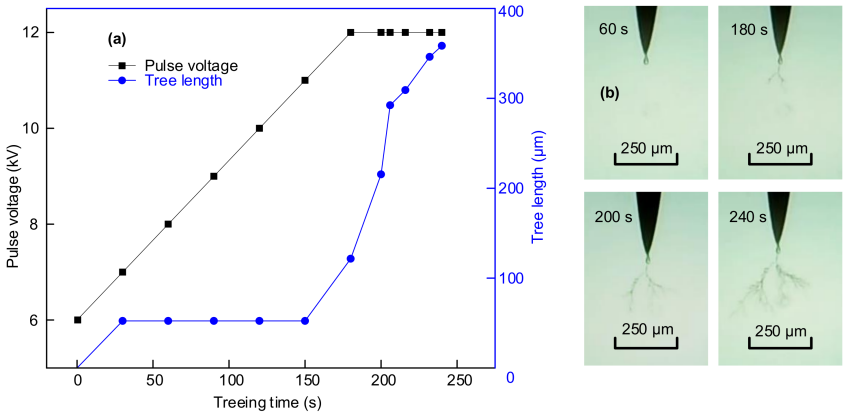

Figure 6. Growth process of bubble tree: (**a**) growth of tree length; (**b**) tree structure at different treeing times.

3.3. Tree Structure

There were two types of electrical trees at 60 min. Figure 7a,b show branch-like trees and Figure 7c,d show pine-like trees. The branch tree has a simple structure with several obvious main long branches. However, the main branch is not obvious in the pine structure and there are a lot of crooked tiny branches in the whole area. Trees under pulse voltage of ±15 kV combined with DC from

−20 to 20 kV were recorded and the tree structure distribution is shown in Table 1. It can be seen that the branch-like tree only exists under positive pulse voltage and the pine tree appears when the pulse is negative. It should also be noted that breakdown happens when the peak value of combined voltage is 35 kV or −35 kV.

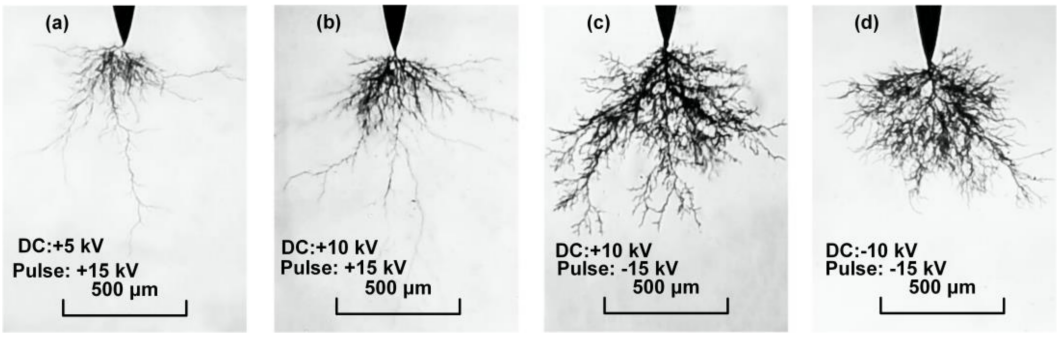

Figure 7. Typical trees at 60 min: (**a**,**b**) branch like tree; (**c**,**d**) pine-like tree.

Table 1. Tree structure distribution under different combined voltages at 60 min.

Type	DC (kV)	Pulse (kV)
Branch-like tree	+5 to +15 kV −5 to −20 kV	+15 kV +15 kV
Pine-like tree	−5 to −15 kV +5 to +20 kV	−15 kV −15 kV
Breakdown	+20 kV −20 kV	+15 kV −15 kV

3.4. Tree Length

When the treeing time reached 10 min, the tree length varied under different combined voltages. The tree lengths with different DC and pulse voltages were recorded and are shown in Figure 8.

From Figure 8a, it can be seen that under the −15 kV pulse, tree length varied from 600–1000 μm and trees with negative DC were longer than those with positive. When the pulse voltage changed to positive, trees with positive DC voltage were much longer than those with negative. From the results, it can be concluded that trees under combined voltage with the same polarity are longer. Especially with combined voltage of 20 kV DC and 15 kV pulse, tree breakdown occurs in a short time (less than 10 min). Figure 8b shows the effect of pulse voltage. It indicates that higher pulse accelerates tree growth when DC is constant.

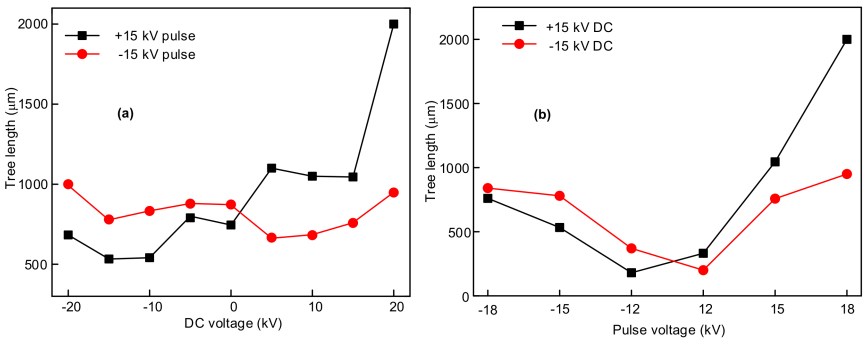

Figure 8. Effect of pulse and DC voltage on tree length: (**a**) tree length under different DC voltages; (**b**) tree length under different pulse voltages.

4. Discussion

4.1. Tree Inception under Combined Voltage

It is known that space charge plays an important role in the tree inception process. Several models for space charge injection have been published. In the field limiting space charge (FLSC) model [33], space charge mobility is assumed to rise sharply from a small value $\delta\mu$ ($\delta << 1$) to a high value μ when the local electric field increases to a constant E_c, as shown in Figure 9. It is assumed that a static space charge region is formed by the charge injection. Its boundary is approximated by the surface where $E = E_c$. In this model, the injected charge density can be calculated using the following [33]:

$$\rho = \frac{2\varepsilon_r \varepsilon_0 E_c}{R} \tag{1}$$

where ε_r is the relative dielectric constant of SIR and R is the curvature radius of the needle tip, 3 μm.

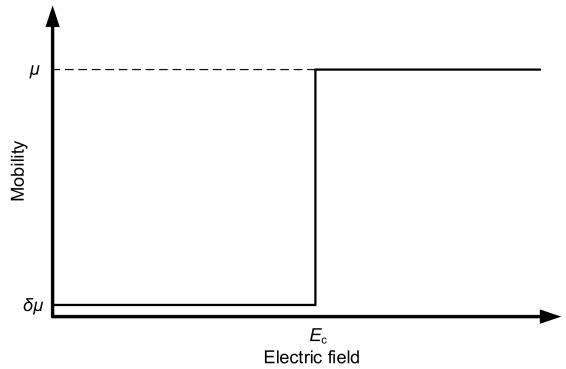

Figure 9. Field-dependent mobility used in the model.

This indicates that with the same R, ρ is constant. The radius of the space charge region can be calculated as follows [33]:

$$R_s = \frac{R(1 + V/V_c)}{2} \tag{2}$$

where R is the curvature radius of the needle tip, V is the voltage of the needle tip and V_c is the critical voltage for space charge formation, which can be assumed to be constant for the same electrodes and insulation.

According to Equation (2), the space charge region size changes with V. This means that during the application of combined voltage, the amount of space charge and size of the space charge region will both change with the voltage.

Figure 10a shows the space charge and electric field distribution under DC, where E_{dc} is the electric field produced by DC voltage and E_{sc} is the electric field produced by space charge. When negative DC is applied via the needle tip, electrons will be injected into the SIR by field emission and the space charge region is formed [34]. With the effect of space charge, there is an inflection point of the field, which exists at the space charge boundary. In previous research, this boundary was calculated to be about 10 μm [34–36]. Previous work [36,37] showed the total electric field around the needle tip under DC, while ϕ_m (work function of the metal needle tip) and χ_I (electron affinity) were not considered in [36]. Taking ϕ_m and χ_I into consideration [13], the field distribution in [36] can be modified as Figure 10(a2), which is the same as in [37]. The field strength at the tip is $E_{in} > 0$. d_o is the distance of space charge boundary from the needle tip and

$$d_o = R_s - R \tag{3}$$

This indicates that d_o can be calculated by Equations (2) and (3).

When a combined voltage of type B is applied, the distribution will be different. Here we analyze the combined voltage with negative DC shown in Figure 2b and the result is shown in Figure 10b. When the negative DC voltage is first applied via the needle electrode, the space charge is injected from the needle tip by field emission. With the pulse voltage in the same polarity, the voltage on the tip will be increased. According to [37–39], the electric field E_{tip} at the needle tip can be calculated by

$$V = \frac{1}{C}E_{\mathrm{tip}} + \frac{k\alpha}{C\varepsilon_0\varepsilon_{\mathrm{r}}}\exp(\beta E_{\mathrm{tip}}) \tag{4}$$

where C is constant, k is a dimensionless constant determined by the sample geometry and the space charge injection depth and α and β are constants depending on the temperature and potential barrier height. It can be seen that E_{tip} increases with increasing V. This will make the electric field near the needle tip increase by ΔE, which can be considered to be caused by the pulse voltage. In Figure 10(b2), ΔE is shown as E_{p}. This makes the total electric field E increase in the space charge region, which can be calculated roughly as:

$$E = E_{\mathrm{dc}} + E_{\mathrm{p}} - E_{\mathrm{sc}} \tag{5}$$

With the E_{tip} higher than E_{in}, more electrons will be injected into SIR as a result. The space charge region boundary will extend because of the rising V, while after the falling edge, it turns back to d_o. The change of space charge boundary and reinjection indicate the movement of space charge. Some hot electrons will get high kinetic energy because of the increased electric field. Meanwhile, the trapped electrons will get the energy to detrap, releasing the accumulated electrical–mechanical energy [40]. This energy may break the molecular chain and lead to tree inception. With different DC voltages, there will be different amounts of injected space charge [33]. However, tree initiation is only related to effective collision with enough energy. As a result, with different negative DC, the negative inception pulse does not obviously change. The same result exists under combined voltage of positive DC and positive pulse.

When pulse voltage with the opposite polarity is applied, the mechanism of tree inception will be different. Tree inception under negative DC and positive pulse (type C, as shown in Figure 2c) is discussed here. During the experiment, negative DC voltage was applied first, the electrons were injected and the distribution was similar to what was discussed above. When a positive pulse voltage was applied later, the distribution of combined electric field around the needle tip changed, as shown in Figure 10c. With the decreased V, the electric field $E_{\mathrm{dc}} + E_{\mathrm{p}}$ caused by the combined voltage decreased rapidly. E_{sc} may be higher than $E_{\mathrm{dc}} + E_{\mathrm{p}}$ at the needle tip. Then E near the needle tip will be changed into the direction opposite to that in Figure 10a,b, as shown in Figure 10(c2). At this time, electric field distribution was similar to the situation of a grounded DC tree [15,16,40]. As a result, electrons near the needle tip will be under field stress toward the needle tip. They will be "extracted" from SIR, similar to the electron extraction under AC voltage. On the falling edge, electrons will be reinjected with the increase of electric field. This injection-extraction of electrons will cause a molecular break and produce a degradation region. Once it is large enough, a partial discharge will occur and an electrical tree will be generated.

However, when the pulse amplitude is higher than the DC voltage in heteropolarity (type D, as shown in Figure 2d), the combined voltage will trigger an electrical tree as AC voltage, which has been researched in previous papers. Its mechanism is illustrated in Figure 10d. There are positive and negative phases under this voltage. In the positive phase, the electric field of the tip will inject holes into the SIR, forming a positive space charge region around the needle tip and the electric field will change, as shown in Figure 10(d2). The peak value of the electric field appears at d_1, which is the boundary of positive space charge region. The holes and electrons will recombine here and release energy. This energy will also contribute to the tree inception.

Figure 4 shows typical initial trees under different voltages. The initial tree under positive pulse has more channels. According to the previous discussion, it can be seen that the dynamic characteristics of space charge are the main reason for the tree inception under combined voltage. The negative pulse

voltage applied via needle electrode will make the injected electrons move forward from near the tip. When the electrons get enough kinetic energy during this process, the collision will break the molecular chain and cause degradation near the needle tip. Besides, the electrical–mechanical energy released by detrapped electrons will also accelerate the degradation. In this area, injected charges are easier to accumulate and cause partial discharge. Because of the steep electric field gradient, this degradation may only occur near the needle tip. When partial discharge with enough energy occurs in this region, an initial tree with a single channel will be observed. However, the positive pulse voltage will attract the injected electrons back to the needle tip. In this stage, the kinetic energy and electrical-mechanical energy will also cause degradation, which may occur in several regions away from the needle tip. More than one channel may be formed in these regions. As a result, an initial tree with several channels in these regions will be observed.

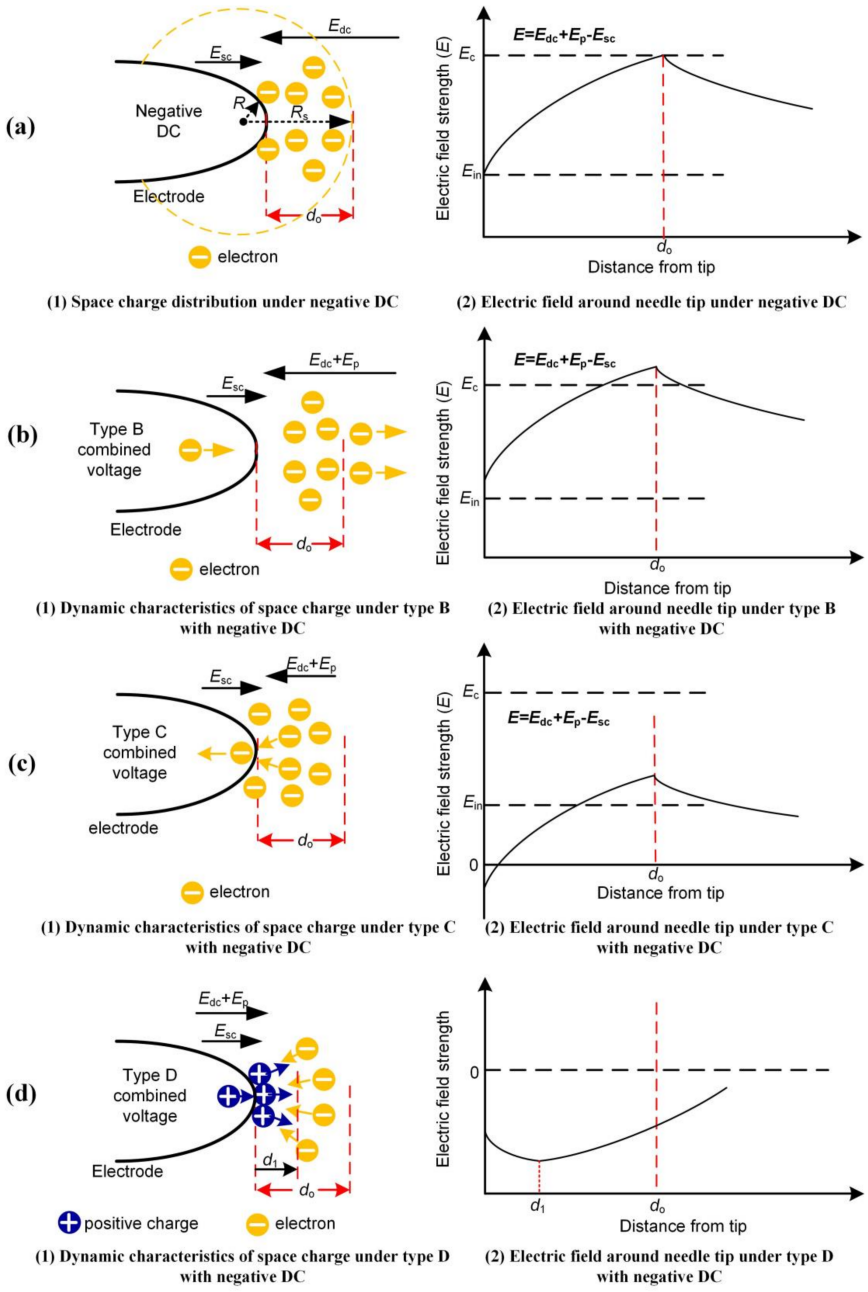

Figure 10. (**a**–**d**) Dynamic characteristics of space charge and electric field under negative DC and combined voltage of types B–D with negative DC, respectively.

4.2. Effects of Different Prestressing Times

In the experiment, it was found that prestressing time had an obvious effect on tree inception characteristics. Figure 5 shows that the inception pulse voltage decreases with the prestressing time of DC in the same polarity. This is because the initial bubble tree shown in Figure 6 occurred under a lower pulse voltage. The probability of an initial bubble tree with different prestressing times is shown in Tables 2 and 3.

Table 2. Probability of bubble tree under different combined voltage with 10 min prestressing DC.

Probability of Bubble Tree	Combined Voltage
70%	Negative pulse and −15 kV DC
12.5%	Positive pulse and −15 kV DC
75%	Positive pulse and +15 kV DC
15%	Negative pulse and +15 kV DC

Table 3. Probability of bubble tree under different combined voltages with 60 min prestressing DC.

Probability of Bubble Tree	Combined Voltage
85%	Negative pulse and −15 kV DC
20%	Positive pulse and −15 kV DC
90%	Positive pulse and +15 kV DC
20%	Negative pulse and +15 kV DC

It is clear that the bubble tree probability with the same polarity DC is higher than that with heteropolarity DC. As shown in Figure 6, a bubble tree was initiated at a much lower pulse than the condition without prestressing. When the traditional tree generated from the bubble, its volume obviously decreased. It can be assumed that in the bubble stage, there is a lot of gas inside it [41] and the different probabilities of bubble tree can be explained by the inception mechanism shown in Figure 11.

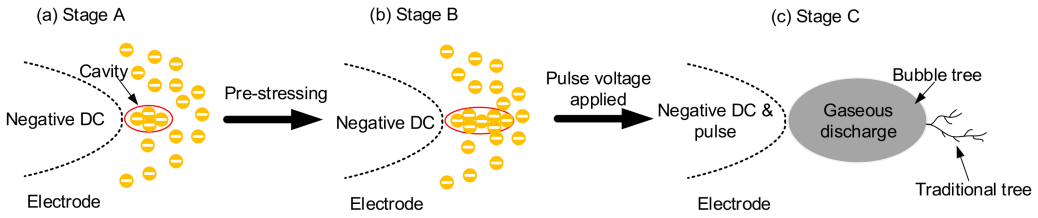

Figure 11. Bubble tree inception with prestressing DC: (**a**–**c**) stages A, B and C of bubble tree inception, respectively.

There may be some small cavities near the needle tip for two reasons: (1) the high Maxwell compressive force caused by the prestressing DC; or (2) different thermal expansion of SIR and needle tip [34]. These small cavities will lead to the accumulation of space charges in the prestressing time, as shown in Figure 11a. When the local electric field inside the cavity is high enough for the discharge, the cavity will be enlarged by this partial discharge of low density. Then the space charges will reaccumulate in the larger cavity and cause another discharge. This stage is shown in Figure 11b. However, this partial discharge does not have enough energy to initiate a tree channel in a short time, because no observable tree appears in 60 min prestressing time.

After the prestressing process, pulse voltage is applied. When the pulse voltage is in the same polarity, the electric field inside the cavity will increase rapidly. More molecular chains will be broken and a large amount of gas will be generated in the cavity. The high gas pressure will enlarge the cavity

to longer than 20 μm, which can be observed as a bubble tree. If the internal pressure produced by the gas is not enough to overcome the external pressure of this bubble, stagnation will occur, as shown in Figure 6a. A traditional tree will propagate from the bubble edge when a higher pulse voltage is applied to cause more intensive gaseous discharge. This process is shown in Figure 11c.

When the pulse voltage is in heteropolarity, the electric field inside the cavity will not increase as previously. Most of the trees will still be initiated by the space charge movement, as discussed in Section 4.1 and there is no obvious decrease in inception pulse voltage. The cavity enlarged in the prestressing stage does not have an obvious promotion effect on tree inception. However, there are still several bubble trees observed under this condition. This may be because the cavity becomes large enough for a gaseous discharge under low voltage.

5. Conclusions

Tree initiation and growth characteristics under combined voltage were investigated. It shows that electrical tree is still a threat to HVDC cable because the existence of this combined voltage. The results can be useful for the manufacture and operation of HVDC cable. The tree initiation mechanism is different from that under DC and analyzed by using the FLSC model. The following are the main conclusions.

(1) Tree inception pulse voltage increased with combined DC when they were in different polarities, while there was no obvious change in inception pulse voltage if the two voltages were in the same polarity. The different initiation mechanisms under different combined voltages led to this result.
(2) The initial tree structure was recorded and the results indicate that it is determined by the pulse polarity. The initial tree structure under positive pulse had a more complex structure, while there was only a single channel under negative pulse.
(3) Two typical trees were observed in the experiment: branch-like trees and pine-like trees. Branch-like trees occurred under positive pulse, while pine-like trees occurred under negative pulse. DC with the same polarity as the pulse accelerates tree growth; tree length will increase with pulse if DC is constant.
(4) Inception pulse voltage decreased with prestressing time when the combined DC was in the same polarity, while under heteropolarity DC, there was no significant change in inception pulse voltage. A special bubble tree was found after the prestressing DC and it may be the result of gas accumulation in the prestressing stage.

Acknowledgments: This work was supported by the National Natural Science Foundation of China (Grant Nos. 51707132, 51677128).

Author Contributions: Tao Han and Boxue Du designed the experiment; Tao Han and Jingang Su performed the experiment, analyzed the data and wrote the paper.

Conflicts of Interest: The authors declare no conflict of interest.

References

1. Fabiani, D.; Montanari, G.C.; Laurent, C.; Teyssedre, G. Polymeric HVDC cable design and space charge accumulation. Part 1: Insulation/semicon interface. *IEEE Electr. Insul. Mag.* **2007**, *23*, 11–19. [CrossRef]
2. Du, B.X.; Hang, X.; Jin, L.; Li, Z.L. Space Charge behaviors of pp/poe/zno nanocomposites for HVDC cables. *IEEE Trans. Dielectr. Electr. Insul.* **2016**, *23*, 3165–3174. [CrossRef]
3. Delpino, S.; Fabiani, D.; Montanari, G.C.; Laurent, C. Polymeric HVDC cable design and space charge accumulation. Part 2: Insulation Interfaces. *IEEE Electr. Insul. Mag.* **2008**, *24*, 14–24. [CrossRef]
4. Zhou, Y.; He, J.L.; Hu, J.; Huang, X.Y.; Jiang, P.K. Evaluation of polypropylene/polyolefin elastomer blends for potential recyclable HVDC cable insulation applications. *IEEE Trans. Dielectr. Electr. Insul.* **2015**, *22*, 673–681. [CrossRef]

5. Källstrand, B.; Borg, D.; Walfridsson, L.; Johansson, K.; Doiron, C.; Fälth, F.; Saltzer, M. DC field distribution around an HVDC cable termination. In Proceedings of the 2015 IEEE Conference on Electrical Insulation and Dielectric Phenomena, Ann Arbor, MI, USA, 18–21 October 2015; pp. 1–4.
6. Zha, J.W.; Wu, Y.H.; Wang, S.J.; Wu, D.H.; Yan, H.D.; Dang, Z.M. Improvement of space charge suppression of polypropylene for potential application in HVDC cables. *IEEE Trans. Dielectr. Electr. Insul.* **2016**, *23*, 2337–2343. [CrossRef]
7. Danikas, M.; Tanaka, T. Nanocomposites-a review of electrical treeing and breakdown. *IEEE Electr. Insul. Mag.* **2009**, *25*, 19–25. [CrossRef]
8. Kurnianto, R.; Murakami, Y.; Hozumi, N.; Nagao, M. Some fundamentals on treeing breakdown in inorganic-filler/LDPE nano-composite material. *IEEE Trans. Dielectr. Electr. Insul.* **2001**, *17*, 685–693.
9. Varlow, B.R.; Auckland, D.W. Mechanical aspects of electrical treeing in solid insulation. *IEEE Electr. Insul. Mag.* **1996**, *12*, 21–26. [CrossRef]
10. Laurent, C.; Massines, F.; Mayoux, C. Optical emission due to space charge effects in electrically stressed polymers. *IEEE Trans. Dielectr. Electr. Insul.* **1997**, *4*, 585–603. [CrossRef]
11. Liu, Y.; Cao, X.L. Electrical tree initiation in XLPE cable insulation by application of DC and impulse voltage. *IEEE Trans. Dielectr. Electr. Insul.* **2013**, *20*, 1691–1698.
12. Saito, Y.; Fukuzawa, M.; Nakamura, H. On the mechanism of tree initiation. *IEEE Trans. Electr. Insul.* **1977**, *EI-12*, 31–34. [CrossRef]
13. Dissado, L.A.; Fothergill, J.C. *Electrical Degradation and Breakdown in Polymers*; Peter Peregrinus Ltd.: London, UK, 1992.
14. Shimizu, N.; Laurent, C. Electrical tree initiation. *IEEE Trans. Dielectr. Electr. Insul.* **1998**, *5*, 651–659. [CrossRef]
15. Sekii, Y.; Kawanami, H.; Saito, M.; Sugi, K. DC tree and grounded DC tree in XLPE. In Proceedings of the 2005 IEEE Conference on Electrical Insulation and Dielectric Phenomena, Nashville, TN, USA, 16–19 October 2005; pp. 523–526.
16. Kawanami, H.; Komatsu, I.; Sekii, Y.; Saito, M.; Sugi, K. Effect of antioxidants on DC tree and grounded DC tree in XLPE. *IEEJ Trans. Fundam. Mater.* **2006**, *126*, 363–368. [CrossRef]
17. Ieda, M.; Nawata, M. DC treeing breakdown associated with space charge formation in polyethylene. *IEEE Trans. Electr. Insul.* **1977**, *12*, 19–25. [CrossRef]
18. Liu, Y.; Cao, X.L. Electrical tree growth characteristics in XLPE cable insulation under DC voltage conditions. *IEEE Trans. Dielectr. Electr. Insul.* **2015**, *22*, 3676–3684. [CrossRef]
19. Wang, Y.N.; Li, G.D.; Wu, J.D.; Yin, Y. Effect of temperature on space charge detrapping and periodic grounded DC tree in cross-linked polyethylene. *IEEE Trans. Dielectr. Electr. Insul.* **2016**, *23*, 3704–3711. [CrossRef]
20. Liu, Y.; Xiao, Y.; Su, Y.; Chen, X.; Zhang, C.; Li, W.P. Electrical treeing test of DC cable XLPE insulation under DC voltage and high temperature. In Proceedings of the 2016 IEEE International Conference on Dielectrics, Montpellier, France, 3–7 July 2016; pp. 752–755.
21. Zhang, Y.X.; Zhou, Y.X.; Chen, M.; Zhang, L.; Zhang, X.; Sha, Y.C. Electrical tree initiation in silicone rubber under DC and polarity reversal voltages. *J. Electrost.* **2017**, *88*, 207–213. [CrossRef]
22. Iddrissu, I.; Zheng, H.L.; Rowland, S.M. Electrical tree growth in epoxy resin under DC voltages. In Proceedings of the 2016 IEEE International Conference on Dielectrics, Montpellier, France, 3–7 July 2016; pp. 820–823.
23. Lu, W.X.; Ooi, B.T. DC overvoltage control during loss of converter in multiterminal voltage-source converter-based HVDC (M-VSC-HVDC). *IEEE Trans. Power Del.* **2003**, *18*, 915–920.
24. Zhou, C.H.; Wang, P. A study of temporary overvoltage at HVDC rectifier stations. In Proceedings of the 2011 IEEE Electrical Power and Energy Conference, Winnipeg, MB, Canada, 3–5 October 2011; pp. 211–215.
25. Hingorani, N.G. Transient overvoltage on a bipolar HVDC overhead line caused by DC line faults. *IEEE Trans. Power Appar. Syst.* **1970**, *PAS-89*, 592–610. [CrossRef]
26. Du, B.X.; Li, Z.L.; Li, J. Effects of direct fluorination on space charge accumulation in HTV silicone rubber. *IEEE Trans. Dielectr. Electr. Insul.* **2016**, *23*, 2353–2360. [CrossRef]
27. Chen, G.; Hao, M.; Xu, Z.Q.; Vaughan, A.; Cao, J.Z.; Wang, H.T. Review of high voltage direct current cables. *CSEE J. Power Energy Syst.* **2015**, *1*, 9–21. [CrossRef]

28. Stancu, C.; Notingher, P.V.; Notingher, P.; Lungulescu, M. Space charge and electric field in thermally aged multilayer joints model. *IEEE Trans. Dielectr. Electr. Insul.* **2016**, *23*, 633–644. [CrossRef]
29. Du, B.X.; Han, T.; Su, J.G. Tree characteristics in silicone rubber/SiO_2 nanocomposites under low temperature. *IEEE Trans. Dielectr. Electr. Insul.* **2014**, *21*, 503–510. [CrossRef]
30. Du, B.X.; Ma, Z.L.; Gao, Y.; Han, T. Effect of ambient temperature on electrical treeing characteristics in silicone rubber. *IEEE Trans. Dielectr. Electr. Insul.* **2011**, *18*, 401–407. [CrossRef]
31. Du, B.X.; Su, J.G.; Li, J.; Han, T. Effects of mechanical stress on treeing growth characteristics in HTV silicone rubber. *IEEE Trans. Dielectr. Electr. Insul.* **2017**, *24*, 1547–1556. [CrossRef]
32. Du, B.X.; Han, T.; Su, J.G. Effect of low temperature on tree characteristics in silicone rubber with different power frequency. *IEEE Trans. Dielectr. Electr. Insul.* **2014**, *21*, 1880–1886. [CrossRef]
33. Hibma, T.; Zeller, H.R.; Pfluger, P.; Baumann, T. A model for space charge injection in dielectrics. In Proceedings of the 1985 IEEE Conference on Electrical Insulation and Dielectric Phenomena, Amherst, NY, USA, 20–24 October 1985; pp. 259–265.
34. Tanaka, T.; Greenwood, A. Effects of charge injection and extraction on tree initiation in polyethylene. *IEEE Trans. Power Syst.* **1978**, *PAS-97*, 1749–1759. [CrossRef]
35. Andrianjohaninarivo, J.; Wertheimer, M.R.; Yelon, A. Nucleation of electrical trees in polyethylene. *IEEE Trans. Electr. Insul.* **1988**, *22*, 709–714.
36. Kosaki, M.; Shimizu, N.; Horii, K. Treeing of polyethylene at 77 K. *IEEE Trans. Electr. Insul.* **1977**, *EI-12*, 40–45. [CrossRef]
37. Alison, J.M.; Champion, J.V.; Dodd, S.J.; Stevens, G.C. Dynamic bipolar charge recombination model for electroluminescence in polymer based insulation during electrical tree initiation. *J. Phys. D Appl. Phys.* **1995**, *28*, 1693–1701. [CrossRef]
38. Hare, R.W.; Hill, R.M.; Budd, C.J. Modelling charge injection and motion in solid dielectrics under high electric field. *J. Phys. D Appl. Phys.* **1993**, *26*, 1084–1093. [CrossRef]
39. Zhang, Y.X.; Zhang, L.; Zhou, Y.X.; Chen, M.; Huang, M.; Liu, R. Temperature dependence of DC electrical tree initiation in silicone rubber considering defect type and polarity. *IEEE Trans. Dielectr. Electr. Insul.* **2017**, *24*, 2694–2702. [CrossRef]
40. Wang, Y.; Guo, F.; Wu, J.; Yin, Y. Effect of DC prestressing on periodic grounded DC tree in cross-linked polyethylene at different temperatures. *IEEE Access* **2017**, *5*, 25876–25884. [CrossRef]
41. Zhang, Y.X.; Zhou, Y.X.; Zhang, L.; Zhou, Z.L.; Nie, Q. Electrical trees and their growth in silicone rubber at various voltage frequencies. *Energies* **2018**, *11*, 327. [CrossRef]